

A Robust Nonlinear RLS Type Adaptive Filter for Second-Order-Intermodulation Distortion Cancellation in FDD LTE and 5G Direct Conversion Transceivers

Andreas Gebhard*, Oliver Lang[‡], Michael Lunglmayr[‡], Christian Motz*
Ram Sunil Kanumalli[†], Christina Auer*, Thomas Paireder*, Matthias Wagner*,
Harald Pretl^{§†} and Mario Huemer* * Christian Doppler Laboratory for Digitally

Assisted RF Transceivers for Future Mobile Communications,

Institute of Signal Processing, Johannes Kepler University, Linz, Austria

[‡]Institute of Signal Processing, Johannes Kepler University, Linz, Austria

[†]Danube Mobile Communications Engineering GmbH & Co KG, Freistädter
Straße 400, 4040 Linz, Austria [§] Institute for Integrated Circuits, Johannes Kepler
University, Linz, Austria Email: andreas.gebhard@jku.at

Abstract

Transceivers operating in frequency division duplex experience a transmitter leakage (TxL) signal into the receiver due to the limited duplexer stop-band isolation. This TxL signal in combination with the second-order nonlinearity of the receive mixer may lead to a baseband (BB) second-order intermodulation distortion (IMD2) with twice the transmit signal bandwidth. In direct conversion receivers, this nonlinear IMD2 interference may cause a severe signal-to-interference-plus-noise ratio degradation of the wanted receive signal. This contribution presents a nonlinear Wiener model recursive-least-squares (RLS) type adaptive filter for the cancellation of the IMD2 interference in the digital BB. The included channel-select-, and DC-notch filter at the output of the proposed adaptive filter ensure that the provided IMD2 replica includes the receiver front-end filtering. A second, robust version of the nonlinear RLS algorithm is derived which provides numerical stability for highly correlated input signals which arise in e.g. LTE-A intra-band multi-cluster transmission scenarios. The performance of the proposed algorithms is evaluated by numerical simulations and by measurement data.

Index terms — second-order intermodulation, self-interference, adaptive filters, interference cancellation, LTE-A, 5G, RLS

I. INTRODUCTION

Modern radio frequency (RF) transceivers are enhanced by digital signal processing to mitigate non-idealities in the analog front-end. One of the main reasons of receiver desensitization in frequency division duplex (FDD) transceivers is the limited duplexer isolation between the transmitter and the receiver which is around 50 dB to 55 dB [1,2]. The resulting transmitter leakage (TxL) signal can be identified as the root cause of several receiver baseband (BB) interferences. Especially in carrier aggregation (CA) receivers multiple clock sources are needed to cover the different CA scenarios and band combinations. Due to cross-talk between the receivers on the chip and device nonlinearities, spurs appear in the receiver front-end.

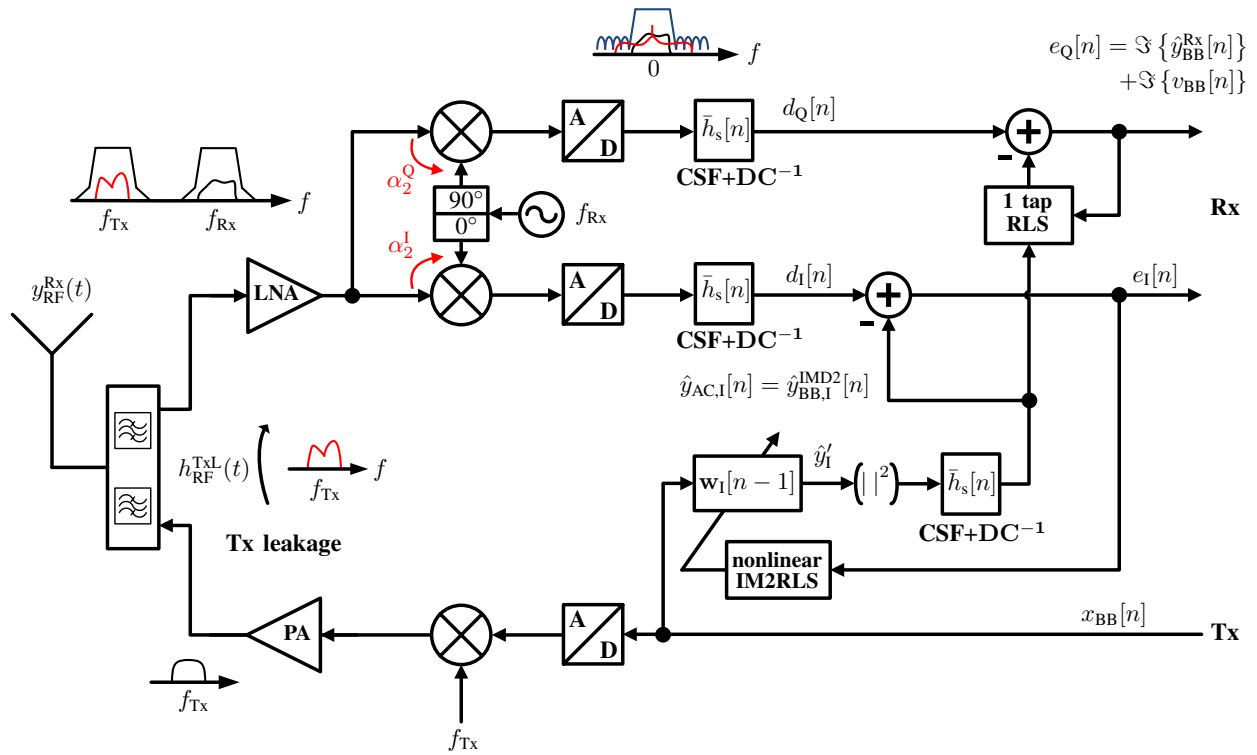


Fig. 1. Block diagram depicting an RF transceiver operating in FDD mode which experiences a second-order intermodulation distortion in the receiver due to the transmitter leakage signal and the Rx mixer RF-to-LO terminal coupling. A nonlinear RLS-type adaptive filters is used to estimate the I-path IMD2 interference. The Q-path IMD2 interference is estimated with a linear 1-tap RLS adaptive filter which uses the estimated I-path IMD2 replica as reference input.

If such a spur falls near the actual transmit (Tx) frequency, then the TxL signal is down-converted into the Rx BB where it causes a signal-to-interference-plus-noise ratio (SINR) degradation of the wanted receive signal. The cancellation of this so called modulated spurs with adaptive filtering is demonstrated in [3,4].

Another prominent interference caused by the TxL signal and the second-order nonlinearity of the receiver is the second-order intermodulation distortion (IMD2). This second-order nonlinear distortion is caused by e.g. a coupling between the RF- and LO-ports in the I-, and Q-path of the Rx IQ-mixer as indicated in Fig. 1 [5]. An interesting fact of this nonlinear interference is, that one part of the generated second-order intermodulation products always falls around zero-frequency independent of the Tx-to-Rx frequency offset (duplexing distance). In case of direct-conversion receiver architectures, this leads to a degradation of the wanted receive signal.

The mathematical modeling in [6,7] shows that the BB IMD2 interference contains the squared envelope of the BB equivalent TxL signal. The resulting BB IMD2 interference has twice the Tx signal bandwidth and contains a DC due to the envelope-squaring. In the receiver front-end, the overall DC arising from a number of sources is canceled by a mixed-signal cancellation to prevent the analog-to-digital converter (ADC) from saturation. In the digital domain, the signal is filtered by a channel-select filter (CSF) to reduce its bandwidth to the Long Term Evolution (LTE) signal bandwidth.

In the existing literature, the authors of [8]–[10] discussed adaptive least-mean-squares (LMS) type IMD2 interference cancellation algorithms for frequency-flat duplexer stop-bands. In [11] a Volterra kernel based least-squares (LS) approach for frequency-selective Tx-Rx responses is proposed. The authors in [7] presented a two-step LS approach for the IMD2 cancellation and considered a static 3rd-order power amplifier (PA) nonlinearity and IQ-imbalance in the transmit mixer. In [12] a Tx CA transceiver is considered where the transmit signal of both transmitters leaks through a diplexer into one unpaired CA receiver. The diplexer stop-band is modeled as a first-order finite impulse response (FIR) system which states a nearly frequency-flat response. The authors incorporated a fourth-order nonlinearity without memory into the estimation process, which results in an LS problem with four unknown coefficients.

This contribution presents a nonlinear Wiener model RLS type adaptive filter (IM2RLS) with exponential forgetting factor which is suitable for highly frequency selective duplexer stop-band frequency responses like indicated in Fig. 2. It targets the digital IMD2 cancellation for high performance cellular base stations and mobile phones. The Wiener model uses a static

nonlinearity at the output of the adaptive filter which has the advantage that less coefficients are needed in the estimation process compared to a Volterra kernel based adaptive filter [13].

An additional version of the proposed algorithm is presented which enhances the algorithm by a DC-notch filter to cancel the DC in the interference replica. This is needed because direct-conversion receivers employ a DC cancellation to suppress the DC in order to prevent the ADC from saturation. The DC in the received signal is time-variant and has many sources like e.g. LO-LO self mixing [5], and therefore must not be related explicitly to the DC which is generated by the IMD2 interference. Consequently, the IMD2 interference related DC is removed from the received signal which complicates the IMD2 replica estimation. This DC removal is considered in [6,11], and neglected in [7]–[9,14].

The derived IM2RLS with DC-notch filter is extended by a regularization (R-IM2RLS) which makes the algorithm applicable for highly correlated BB transmit signals where the autocorrelation matrix can be close to singular. A high correlation in the transmit signal can be due to oversampling which happens e.g. in the case of multi-cluster transmissions (introduced in 3GPP LTE-A Release 11) where only a part of the available resource blocks (RBs) are allocated. The presented IM2RLS algorithm is an extension to the nonlinear LMS type adaptive filter derived in [6] with improved steady-state cancellation and convergence speed.

The structure of the presented work is as follows: Section II explains the second-order input intercept point (IIP2) characterization and demonstrates the degradation of the Rx performance due to the IMD2 interference. Section III provides a detailed IMD2 interference model which motivates the proposed structure of the nonlinear adaptive filter. In Section IV, the IM2RLS algorithm is derived and the impact of adding a DC-notch filter to the algorithm is evaluated. The R-IM2RLS algorithm is derived in section V which is robust against highly correlated input signals as they occur in intra-band multi-cluster transmissions. Finally, in the sections VI and VII, the performance of the R-IM2RLS algorithm is evaluated with simulations and measured data using RF components.

II. PROBLEM STATEMENT

The receiver IIP2 is characterized by using two cosine signals with the frequencies f_1 and f_2 of equal amplitude and the total power $P_{in,2t}$ at the input of the nonlinear mixer. The resulting total IMD2 power generated at DC, $f_1 + f_2$ and $f_2 - f_1$ at the output of the mixer can be calculated by $P_{IM2}^{Tot,2t} = 2P_{in,2t} - IIP2_{2t}$ [15], where IIP2 is the two-tone IIP2 value in dBm. Here, half of

the total IMD2 power falls to DC, and one quarter each to $f_1 + f_2$ and $f_2 - f_1$. To characterize the IIP2 in a zero-IF receiver, the frequencies f_1 and f_2 are chosen such that $f_2 - f_1$ falls within the CSF bandwidth. Thereby the power at $f_2 - f_1$ is measured and the IIP2 is determined by
$$\text{IIP2}_{2t} = 2P_{\text{in},2t} - P_{\text{IM2}}^{f_2-f_1} - 6 \text{ dB}.$$

For modulated signals, the BB IMD2 power is modulation dependent and further reduced by the CSF. This is considered by a correction-factor which corrects the IMD2 power calculated by the two-tone formula [16,17].

Although the DC-, and channel-select filtering in the receiver reduces the IMD2 BB interference power by 6 dB in the two-tone signal case [15], and by about 13.4 dB [6,16,17] in the case of modulated Tx signals, the left-over IMD2 interference may lead to a severe signal-to-noise ratio (SNR) degradation of the wanted Rx signal in reference sensitivity cases [18]. Assuming a transmitter power of 23 dBm at the antenna, and an average Tx-to-Rx duplexer isolation at the transmit frequency of 50 dB, the TxL signal power at the input of the receiver is $P_{\text{RF}}^{\text{TxL}} = 23 \text{ dBm} - 50 \text{ dB} = -27 \text{ dBm}$. After amplification with the low noise amplifier (LNA) gain which is assumed as 20 dB, the RF TxL signal power increases to $P_{\text{RF}}^{\text{TxL}} = -7 \text{ dBm}$ at the input of the nonlinear mixer.

The two-tone IIP2 value of typical RF mixers is between 50 dBm and 70 dBm [19,20]. Assuming an IIP2 of 60 dBm, the resulting BB IMD2 power with a full allocated LTE10 QPSK modulated transmission and the determined correction factor of $\text{CF} = 13.4 \text{ dB}$ is

$$P_{\text{IM2}}^{\text{CSF,LTE}} = 2P_{\text{RF}}^{\text{TxL}} - \text{IIP2} - \text{CF} = -87.4 \text{ dBm} \quad [6].$$
 In an LTE10 reference sensitivity case, the wanted signal power at the antenna can be as low as -97 dBm [18]. The thermal noise power within 10 MHz bandwidth is -104.5 dBm and the assumed receiver noise figure (NF) is 4.5 dB which results in a receiver noise floor at -100 dBm. After amplification with 20 dB LNA gain, the wanted signal power is -77 dBm and the noise floor at -80 dBm corresponding to an Rx SNR of 3 dB. The SNR drops from 3 dB to an SINR of 2.27 dB due to the IMD2 interference assuming an IIP2 of +60 dBm. In case of an reduced IIP2 of 55 dBm / 50 dBm, the SINR drops even further to 1 dB / -1.4 dB, respectively. Fig. 2 depicts the spectrum of the frequency selective BB equivalent TxL signal $y_{\text{BB}}^{\text{TxL}}$ which generates the complex valued IMD2 interference $y_{\text{BB}}^{\text{IMD2}}$ by a coupling between the RF-to-LO terminals of the I-, and Q-path mixer. The total received signal $y_{\text{BB}}^{\text{Tot}}$ contains the wanted Rx signal $y_{\text{BB}}^{\text{Rx}}$ which is degraded by the IMD2 interference and the noise.

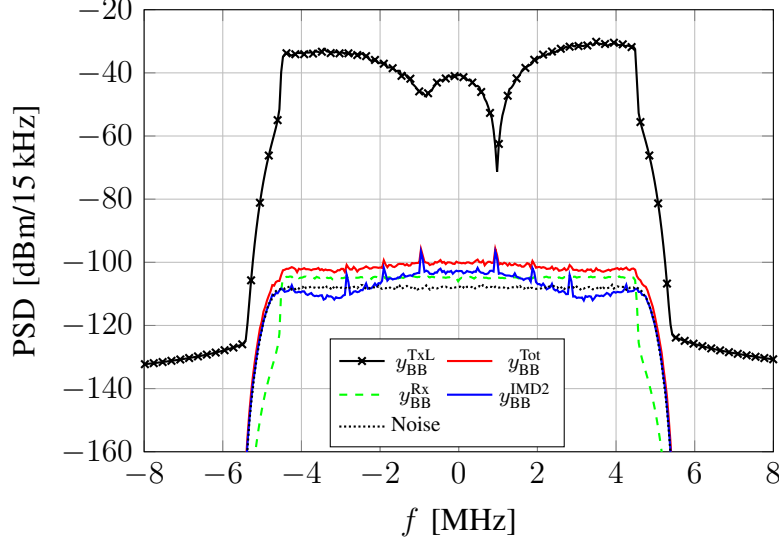


Fig. 2. Equivalent BB spectrum of the frequency-selective Tx leakage signal $y_{\text{BB}}^{\text{TxL}}$ (the corresponding passband signal is located at f_{Tx}) and the total received signal $y_{\text{BB}}^{\text{Tot}}$ after amplification with 20 dB LNA gain. The wanted Rx signal with SNR=3 dB, and the receiver noise floor after amplification with 20 dB LNA gain are at -77 dBm and -80 dBm $\hat{=}$ -108.2 dBm/15 kHz respectively. The total received signal contains the DC-, and channel-select filtered IMD2 interference with $P_{\text{Tx}} = 23$ dBm at an assumed IIP2 of 50 dBm.

III. SYSTEM MODEL

A. IMD2 Interference Model

Based on the block diagram in Fig. 1 depicting an RF transceiver operating in FDD mode, a detailed IMD2 interference model is derived. The used mathematical operators $(\cdot)^*$, $(\cdot)^T$, $(\cdot)^H$, and $*$ denote the complex conjugate, transpose, Hermitian transpose, and convolution, respectively. The complex BB transmit signal $x_{\text{BB}}(t) = x_{\text{I}}(t) + jx_{\text{Q}}(t)$ is up-converted to the passband and amplified by the linearly assumed PA with gain A_{PA} resulting in the RF transmit signal

$$x_{\text{RF}}(t) = A_{\text{PA}} \Re \{ x_{\text{BB}}(t) e^{j2\pi f_{\text{Tx}} t} \}. \quad (1)$$

This signal leaks through the duplexer RF stop-band impulse response

$$h_{\text{RF}}^{\text{TxL}}(t) = 2\Re \{ h_{\text{BB}}^{\text{TxL}}(t) e^{j2\pi f_{\text{Tx}} t} \}, \quad (2)$$

which is modeled by the BB equivalent duplexer impulse response $h_{\text{BB}}^{\text{TxL}}(t)$ into the receiver, thereby creating the TxL signal

$$\begin{aligned} y_{\text{RF}}^{\text{TxL}}(t) &= x_{\text{RF}}(t) * h_{\text{RF}}^{\text{TxL}}(t) \\ &= A_{\text{PA}} \Re \{ [x_{\text{BB}}(t) * h_{\text{BB}}^{\text{TxL}}(t)] e^{j2\pi f_{\text{Tx}} t} \}. \end{aligned} \quad (3)$$

The received signal at the output of the LNA with gain A_{LNA}

$$y_{\text{RF,LNA}}^{\text{Tot}}(t) = A_{\text{LNA}} [y_{\text{RF}}^{\text{TxL}}(t) + y_{\text{RF}}^{\text{Rx}}(t) + v_{\text{RF}}(t)], \quad (4)$$

is composed by the amplified TxL signal, the wanted Rx signal $y_{\text{RF}}^{\text{Rx}}(t)$ and the noise signal $v_{\text{RF}}(t)$. The output signal of the I-, and Q-path mixer is combined into the complex valued signal $y_{\text{RF,mixer}}^{\text{Tot}}(t)$ (5). It contains the wanted signal which is down-converted with the linear gain $\alpha_1 = \alpha_1^{\text{I}} + j\alpha_1^{\text{Q}}$, and the second order interference with the mixer RF-to-LO terminal coupling coefficient $\alpha_2 = \alpha_2^{\text{I}} + j\alpha_2^{\text{Q}}$.

$$\begin{aligned} y_{\text{RF,mixer}}^{\text{Tot}}(t) &= y_{\text{RF,LNA}}^{\text{Tot}}(t)\alpha_1^{\text{I}} \cos(2\pi f_{\text{Rx}}t) \\ &\quad + y_{\text{RF,LNA}}^{\text{Tot}}(t) [\alpha_2^{\text{I}} y_{\text{RF,LNA}}^{\text{Tot}}(t)] \\ &\quad - jy_{\text{RF,LNA}}^{\text{Tot}}(t)\alpha_1^{\text{Q}} \sin(2\pi f_{\text{Rx}}t) \\ &\quad + jy_{\text{RF,LNA}}^{\text{Tot}}(t) [\alpha_2^{\text{Q}} y_{\text{RF,LNA}}^{\text{Tot}}(t)] \\ &= y_{\text{RF,LNA}}^{\text{Tot}}(t)\alpha_1 e^{-j2\pi f_{\text{Rx}}t} + \alpha_2 y_{\text{RF,LNA}}^{\text{Tot}}(t)^2 \end{aligned} \quad (5)$$

Assuming a direct conversion receiver, and using the identity $\Re\{\eta e^{j\kappa}\} = \frac{1}{2}(\eta e^{j\kappa} + \eta^* e^{-j\kappa})$, the total mixer output signal by neglecting the signal content which falls outside the BB bandwidth becomes

$$\begin{aligned} y_{\text{RF,mixer}}^{\text{Tot}}(t) &= \alpha_1 \frac{A_{\text{LNA}}}{2} y_{\text{BB}}^{\text{Rx}}(t) + \alpha_1 \frac{A_{\text{LNA}}}{2} v_{\text{BB}}(t) \\ &\quad + \frac{\alpha_2}{2} \cdot \left(|A_{\text{LNA}} A_{\text{PA}} x_{\text{BB}}(t) * h_{\text{BB}}^{\text{TxL}}(t)|^2 + \frac{1}{2} |y_{\text{BB}}^{\text{Rx}}(t)|^2 \right. \\ &\quad \left. + \Re\{y_{\text{BB}}^{\text{Rx}}(t)v_{\text{BB}}^*(t)\} + \frac{1}{2} |v_{\text{BB}}(t)|^2 \right). \end{aligned} \quad (6)$$

As $|\alpha_2| \ll 1$, the three last terms in (6) may be neglected [6,7]. The total received discrete-time BB signal including the DC-cancellation and channel-select filtering becomes

$$\begin{aligned} y_{\text{BB}}^{\text{Tot}}[n] &= \alpha_1 \frac{A_{\text{LNA}}}{2} y_{\text{BB}}^{\text{Rx}}[n] * \bar{h}_s[n] + \alpha_1 \frac{A_{\text{LNA}}}{2} v_{\text{BB}}[n] * \bar{h}_s[n] \\ &\quad + \underbrace{\frac{\alpha_2}{2} |A_{\text{LNA}} A_{\text{PA}} x_{\text{BB}}[n] * h_{\text{BB}}^{\text{TxL}}[n]|^2 * \bar{h}_s[n]}_{y_{\text{BB}}^{\text{MD}2}[n]}, \end{aligned} \quad (7)$$

where the DC-, and CSF are combined in the impulse response $\bar{h}_s[n] = h_{\text{DC}}[n] * h_s[n]$. Here, $h_{\text{BB}}^{\text{TxL}}[n] = T_s h_{\text{BB}}^{\text{TxL}}(t)|_{t=nT_s}$ is the impulse invariant [21,22], scaled and sampled version of the continuous-time BB duplexer impulse response $h_{\text{BB}}^{\text{TxL}}(t)$.

B. Interference Replica Model

For the adaptive filter development to cancel the IMD2 interference in the digital BB, the interference model (7) is rewritten to the form

$$\begin{aligned}
 y_{\text{BB}}^{\text{Tot}}[n] &= \underbrace{\frac{\alpha_2^{\text{I}}}{2} |A_{\text{LNA}} A_{\text{PA}} x_{\text{BB}}[n] * h_{\text{BB}}^{\text{TxL}}[n]|^2 * \bar{h}_s[n]}_{y_{\text{BB}}^{\text{IMD2,I}}[n]} \\
 &+ j \underbrace{\frac{\alpha_2^{\text{Q}}}{2} |A_{\text{LNA}} A_{\text{PA}} x_{\text{BB}}[n] * h_{\text{BB}}^{\text{TxL}}[n]|^2 * \bar{h}_s[n]}_{y_{\text{BB}}^{\text{IMD2,Q}}[n]} + v'_{\text{BB}}[n]
 \end{aligned} \tag{8}$$

where the complex valued wanted signal and the noise signal are combined in $v'_{\text{BB}}[n]$. Assuming $\alpha_2^{\text{I}} > 0$, and approximating the duplexer impulse response $h_{\text{BB}}^{\text{TxL}}[n]$ by the FIR impulse response vector $\mathbf{h}_{\text{BB}}^{\text{TxL}}$ of length N_{w} , we can rewrite the model (8) further to

$$\begin{aligned}
 y_{\text{BB}}^{\text{Tot}}[n] &= |\mathbf{x}^T[n] \mathbf{h}_{\text{I}}|^2 * \bar{h}_s[n] + j |\mathbf{x}^T[n] \mathbf{h}_{\text{Q}}|^2 * \bar{h}_s[n] + v'_{\text{BB}}[n] \\
 &= y_{\text{BB}}^{\text{IMD2,I}}[n] + j \epsilon y_{\text{BB}}^{\text{IMD2,I}}[n] + v'_{\text{BB}}[n],
 \end{aligned} \tag{9}$$

where \mathbf{h}_{I} and \mathbf{h}_{Q} are incorporating $\mathbf{h}_{\text{BB}}^{\text{TxL}}$ and all scalar scaling factors in the I-, and Q-path respectively. The used vector $\mathbf{x}[n]$ is the complex valued tapped delay-line input signal vector $\mathbf{x}[n] = [x_{\text{BB}}[n], x_{\text{BB}}[n-1], \dots, x_{\text{BB}}[n-N_{\text{w}}+1]]^T$, and the real valued scaling factor ϵ shows that the Q-path IMD2 interference may be modeled as a scaled version of the I-path interference. Motivated by the model (9) we propose the I-path IMD2 interference replica model

$$\hat{y}_{\text{AC,I}}[n] = |\mathbf{x}^T[n] \mathbf{w}_{\text{I}}[n]|^2 * \bar{h}_s[n], \tag{10}$$

using the adaptive filter coefficient vector $\mathbf{w}_{\text{I}}[n]$. The index AC indicates the DC cancellation in the IMD2 replica generation. The replica model comprises an adaptive Wiener model FIR filter where the output signal is DC-, and channel-select filtered. The Q-path IMD2 interference is generated by estimating the scaling parameter ϵ by a linear single-tap RLS algorithm which uses the estimated I-path IMD2 interference as reference input. This model is used to derive the adaptive filter structure shown in Fig. 1 to cancel the IMD2 interference in the digital BB. For the case if $\alpha_2^{\text{I}} < 0$, the sign of the desired signal in the I-path d_{I} and the replica signal of the adaptive filter need to be changed.

IV. NONLINEAR RECURSIVE LEAST-SQUARES ALGORITHM

In this section, a nonlinear Wiener model RLS type adaptive filter to estimate the channel-select filtered I-path IMD2 interference is developed. In a first step the IM2RLS algorithm

without DC-notch filter, which implies that the received signal contains the DC, is developed. Therefore, the replica model (10) without DC cancellation

$$\begin{aligned}\hat{y}_I[n] &= |\mathbf{x}^T[n]\mathbf{w}_I[n]|^2 * h_s[n] \\ &= \mathbf{x}^T[n]\mathbf{w}_I[n]\mathbf{x}^H[n]\mathbf{w}_I^*[n] * h_s[n]\end{aligned}\quad (11)$$

is used. The LS cost function up to the time index n with the exponential forgetting factor $0 \ll \lambda \leq 1$ is

$$J_{\text{LS}}[n] = \sum_{i=0}^n \lambda^{n-i} |d_I[i] - \mathbf{x}^T[i]\mathbf{w}_I[n]\mathbf{x}^H[i]\mathbf{w}_I^*[n] * h_s[i]|^2. \quad (12)$$

This cost function is visualized in Fig. 3 for an example impulse response $\mathbf{h}_I = [1, 0.5]^T$ and $\lambda = 1$ where the estimated coefficients $w_{I,0}$ and $w_{I,1}$ are constrained to be real valued. Two equivalent global minimum points and a local maximum at the origin $\mathbf{w}_I = \mathbf{0}$ can be observed. The two solutions $\mathbf{w}_{I,1} = [1, 0.5]^T$, and $\mathbf{w}_{I,2} = [-1, -0.5]^T$ minimize the cost function which can be explained with the absolute-squaring nature of the IMD2 interference. Both solutions lead to the same IMD2 replica signal. Assuming real valued CSF impulse response coefficients $h_s[n]$,

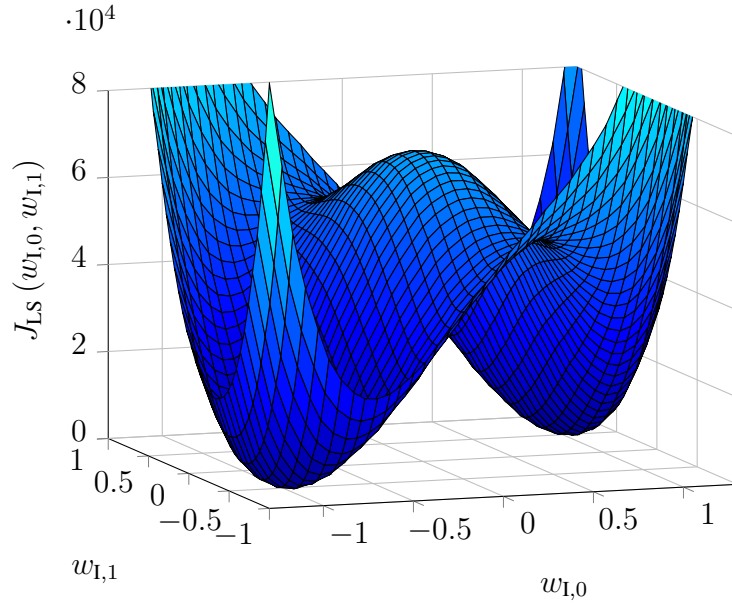


Fig. 3. Shape of the cost function (12) for white Gaussian input signals with $\lambda = 1$ and for the real valued coefficient vector $\mathbf{h}_I = [1, 0.5]^T$ when the desired signal $d_I[n]$ and the IMD2 replica are containing the DC. At the origin $\mathbf{w}_I = \mathbf{0}$, a local maximum can be observed.

and observing that $d_I[i]$ is the desired signal in the I-path, and therefore real valued, the gradient

of the cost function (12) may be derived. The gradient of the cost function with respect to the conjugate coefficient vector \mathbf{w}_1^* using the Wirtinger calculus [23]–[25] becomes

$$\begin{aligned}\nabla_{\mathbf{w}_1^*} J_{\text{LS}} &= \left[\frac{\partial J_{\text{LS}}[n]}{\partial \mathbf{w}_1^*[n]} \right]^T \\ &= \sum_{i=0}^n \lambda^{n-i} \left[-2 d_1[i] \mathbf{x}^T[i] \mathbf{w}_1[n] \mathbf{x}^*[i] * h_s[i] \right. \\ &\quad \left. + 2 \left(\mathbf{x}^T[i] \mathbf{w}_1[n] \mathbf{x}^*[i] * h_s[i] \right) \right. \\ &\quad \left. \cdot \left(\mathbf{x}^H[i] \mathbf{w}_1^*[n] \mathbf{x}^T[i] * h_s[i] \right) \mathbf{w}_1[n] \right].\end{aligned}\quad (13)$$

By setting the gradient to zero, the Wiener Filter equation is obtained by

$$\tilde{\mathbf{R}}(\mathbf{w}_1[n]) \mathbf{w}_1[n] = \tilde{\mathbf{r}}(\mathbf{w}_1[n]), \quad (14)$$

where it can be observed that the autocorrelation matrix $\tilde{\mathbf{R}}$ and the cross-correlation vector $\tilde{\mathbf{r}}$ are functions of the unknown coefficient vector $\mathbf{w}_1[n]$. In a slowly varying or nearly stationary system environment it can be assumed that $\mathbf{x}^T[i] \mathbf{w}_1[n] \approx \mathbf{x}^T[i] \mathbf{w}_1[i-1]$ when the index i is close to n [26,27]. If the index $i \ll n$, the approximation introduces an error which is however attenuated by the forgetting factor. Defining the new cost function

$$\begin{aligned}J'_{\text{LS}}[n] &= \sum_{i=0}^n \lambda^{n-i} |d_1[i] - \mathbf{x}^T[i] \mathbf{w}_1[i-1] \mathbf{x}^H[i] \mathbf{w}_1^*[n] * h_s[i]|^2 \\ &= \sum_{i=0}^n \lambda^{n-i} |d_1[i] - \mathbf{z}^T[i] \mathbf{w}_1^*[n] * h_s[i]|^2 \\ &= \sum_{i=0}^n \lambda^{n-i} |e_1[i]|^2\end{aligned}\quad (15)$$

and introducing the new input vector $\mathbf{z}[i] = \mathbf{x}^T[i] \mathbf{w}_1[i-1] \mathbf{x}^*[i]$, we can overcome this limitation. Following the traditional RLS derivation [28], the IM2RLS algorithm to estimate the I-path IMD2 interference in the digital BB becomes (16)-(20):

$$\hat{y}_1[n] = \mathbf{z}^T[n] \mathbf{w}_1^*[n-1] * h_s[n] \quad (16)$$

$$e_1[n] = d_1[n] - \hat{y}_1[n] \quad (17)$$

$$\mathbf{k}[n] = \frac{\mathbf{P}[n-1] \mathbf{z}_f[n]}{\lambda + \mathbf{z}_f^H[n] \mathbf{P}[n-1] \mathbf{z}_f[n]} \quad (18)$$

$$\mathbf{P}[n] = \frac{1}{\lambda} [\mathbf{P}[n-1] - \mathbf{k}[n] \mathbf{z}_f^H[n] \mathbf{P}[n-1]] \quad (19)$$

$$\mathbf{w}_I[n] = \mathbf{w}_I[n-1] + e_I[n]\mathbf{k}[n] \quad (20)$$

To avoid the channel-select filtering of each element in the vector $\mathbf{z}_f[n] = \mathbf{z}[n] * h_s[n]$ which is mainly necessary to align the signals due to the CSF group delay, we introduce the signals $x_f[n] = x[n] * h_s[n]$ and $y'_f[n] = \mathbf{x}^T[n]\mathbf{w}_I[n-1]$. Using the delay line vector $\mathbf{x}_f[n] = [x_f[n], x_f[n-1], \dots, x_f[n-M+1]]^T$, the vector $\mathbf{z}_f[n]$ may be approximated by $\mathbf{z}_f[n] \approx (y'_f[n] * h_s[n])\mathbf{x}_f^*[n]$. With this formulation, a fractional and non-constant group delay of the CSF may be incorporated. In case if the group delay τ_g is constant, and an integer multiple of the sampling time (as e.g. in linear phase FIR filters), the CSF may be approximated by delaying the signal by $\mathbf{z}_f[n] \approx \mathbf{x}^T[n - \tau_g]\mathbf{w}_I[n-1 - \tau_g]\mathbf{x}^*[n - \tau_g]$. In both approximations, the band-limiting effect of the CSF on $\mathbf{z}_f[n]$ is ignored. However, this may be tolerated because due to the envelope-squaring operation in (11) which doubles the signal bandwidth, anyhow an oversampling factor (OSF) of 2 is mandatory to avoid aliasing. Due to the fact, that the I-, and Q-path IMD2 interference differ only by a real valued scaling factor ϵ as derived in (8), the estimated I-path IMD2 replica may be used as a reference to estimate the Q-path IMD2 replica. This may be done by a linear 1-tap RLS algorithm which uses the estimated I-path replica as reference input signal to estimate the Q-path IMD2 replica. In this case, the 1-tap RLS estimates also a possible sign difference between the I-, and Q-path IMD2 interference. Consequently, only the sign of α_2^I has to be detected during calibration of the receiver which may be done by correlation. The replica signal generation (16) is channel-select filtered which reduces the bandwidth of the replica signal to the bandwidth of the received LTE signal.

A. Second-Order Condition

The complex Hessian [24,29] of the cost function (12) at the coefficient value $\mathbf{w}_I = \mathbf{0}$ becomes

$$\begin{aligned} H_I &= \frac{\partial}{\partial \mathbf{w}_I} \left[\frac{\partial J_{LS}}{\partial \mathbf{w}_I^*} \right]^T \Big|_{\mathbf{w}_I = \mathbf{0}} \\ &= \sum_{i=0}^n \lambda^{n-i} [-2 d_I[i] \mathbf{x}^*[i] \mathbf{x}^T[i] * h_s[i]]. \end{aligned} \quad (21)$$

If the desired signal $d_I[n]$ contains the DC (when the receiver has no DC filtering), then $E\{d_I[n]\} \geq 0$ and the Hessian matrix becomes negative semi-definite like depicted with the local maximum in Fig. 3. The usual choice of the zero-vector as initialization of $\mathbf{w}_I[-1]$ results in a zero-gain vector $\mathbf{k}[n]$ for all n . This is reasoned in the cost function (12) depicted in Fig.

3 which has a local maximum at $\mathbf{w}_I = \mathbf{0}$ and therefore a vanishing gradient. Consequently, the algorithm is initialized with $\mathbf{w}_I[-1] \neq \mathbf{0}$ and the parameters $0 \ll \lambda \leq 1$, and $\mathbf{P}[-1] = \nu \mathbf{I}$ with $\nu > 0$.

B. DC Cancellation

To employ an IMD2 interference replica without DC, the replica signal (16) is filtered by the DC-notch filter (23). The new error signal $e_{AC,I}[n] = d_{AC,I}[n] - \hat{y}_{AC,I}[n]$ with the DC-filtered signals is used in the update equation (27). Here, the introduced index AC indicates the DC filtered signals. The IM2RLS algorithm with DC-suppression can be summarized as (22)-(27):

$$\hat{y}_I[n] = \mathbf{z}^T[n] \mathbf{w}_I^*[n-1] * h_s[n] \quad (22)$$

$$\hat{y}_{AC,I}[n] = a \hat{y}_{AC,I}[n-1] + \hat{y}_I[n] - \hat{y}_I[n-1]. \quad (23)$$

$$e_{AC,I}[n] = d_{AC,I}[n] - \hat{y}_{AC,I}[n] \quad (24)$$

$$\mathbf{k}[n] = \frac{\mathbf{P}[n-1] \mathbf{z}_f[n]}{\lambda + \mathbf{z}_f^H[n] \mathbf{P}[n-1] \mathbf{z}_f[n]} \quad (25)$$

$$\mathbf{P}[n] = \frac{1}{\lambda} [\mathbf{P}[n-1] - \mathbf{k}[n] \mathbf{z}_f^H[n] \mathbf{P}[n-1]] \quad (26)$$

$$\mathbf{w}_I[n] = \mathbf{w}_I[n-1] + e_{AC,I}[n] \mathbf{k}[n] \quad (27)$$

The parameter $0 \ll a < 1$ in (23) determines the sharpness of the DC-notch filter and is chosen as $a = 0.998$. In case of DC filtering in the main receiver $E\{d_I[n]\} = 0$, and the Hessian matrix (21) at $\mathbf{w}_I = \mathbf{0}$ is not positive semi-definite anymore. In this case, the local maximum becomes a saddle-point like depicted in Fig. 4. Using N_{CSF} as the number of coefficients of the CSF impulse response, the computational complexity of the IM2RLS with DC-notch filter is $13N_w^2 + 5N_{CSF} + 20N_w + 1$ real multiplications and $2N_w$ real divisions per iteration.

C. Multiple Solutions of the IM2RLS Algorithm

In the cost function shapes depicted in Fig. 3 and Fig. 4, the estimated impulse response coefficients w_0 and w_1 (omitting the index I for the I-path) are constrained to be real valued. It can be observed that the two solutions $\mathbf{w}_0 = [1, 0.5]^T$, and $\mathbf{w}_1 = [-1, -0.5]^T$ minimize the cost function. The existence of multiple solutions can be explained by the absolute-squaring nature of the IMD2 interference.

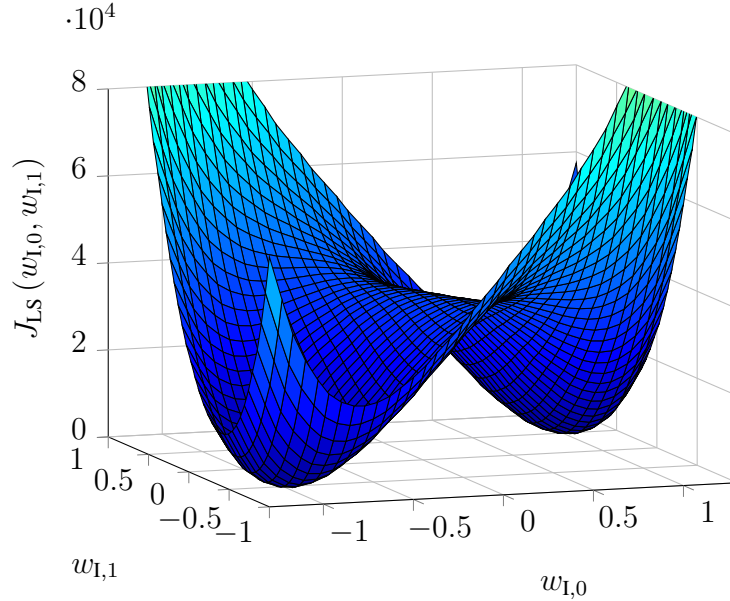


Fig. 4. Shape of the cost function (12) for white Gaussian input signals with $\lambda = 1$ and for the two real valued coefficients $\mathbf{h} = [1, 0.5]^T$. The local maximum at $\mathbf{w}_1 = \mathbf{0}$ (with DC) changed to a saddle-point because the DC filtering is applied.

If the coefficients are allowed to be complex valued, all coefficient pairs $\{w_0, w_1\}$ converge to $|w_0^{\text{end}}| = |h_0|$ and $|w_1^{\text{end}}| = |h_1|$. This scenario is visualized in Fig. 5 where the convergence of the coefficients with the ten different initializations $\mathbf{w}_i[-1] = [1e - 3, 0]^T \exp(j2\pi/10i)$ for $i = 0 \dots 9$ is depicted. Furthermore, each of the estimated coefficient vectors $\mathbf{w}_i^{\text{end}} = [w_{0,i}^{\text{end}}, w_{1,i}^{\text{end}}]^T$ after convergence reach the group delay of the real system impulse response \mathbf{h} .

D. Performance of the IM2RLS with DC Suppression

In this section, the performance of the IM2RLS w/o and w/ DC cancellation is compared. In the first case, the receiver and the IMD2 replica generation of the IM2RLS do not use a DC cancellation. In this hypothetical example it is assumed that the IMD2 interference is the only DC source. In the second case, the receiver uses a DC suppression, and the IM2RLS the DC-notch filter. Both cases are compared within an FDD scenario with full allocated LTE signals using 10 MHz bandwidth, QPSK modulation, short cyclic prefix, and an OSF of 2. The frequency-selective duplexer stop-band impulse response shown in Fig. 6 is used in (7) for the IMD2 interference generation. It is modeled with an FIR system which has 15 complex valued coefficients (on the native LTE10 sampling rate of 15.36 MHz) and a mean Tx-to-Rx isolation of 50 dB [1]. The resulting TxL signal has a strong frequency-selectivity like indicated in Fig. 2. The wanted Rx signal power is at reference sensitivity level $P_{\text{Rx}} = -97$ dBm and the thermal

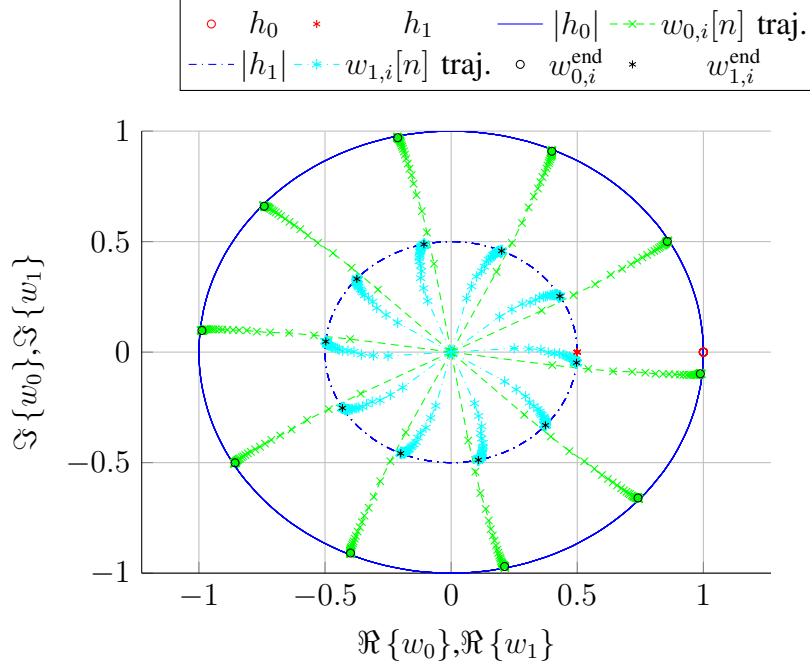


Fig. 5. Illustration of the initialization-dependent multiple solutions where the true coefficient values are $\mathbf{h} = [1, 0.5]^T$. The initial coefficient $w_0[-1]$ is initialized in a 10-point grid around a circle with radius $1e-3$. The initial value of $h_1[-1]$ is always zero. With each initialization, the coefficients converge to the correct absolute value. All ten resulting estimated impulse response vectors \mathbf{w}_i^{end} maintain the same group delay as \mathbf{h} .

noise floor is -104.5 dBm within 10 MHz bandwidth. The receiver NF is 4.5 dB which results in an receiver noise floor of -100 dBm. The LNA gain is 20 dB, and the two-tone mixer IIP2 is 50 dBm. This results in an desensitization of the wanted Rx signal from an SNR = 3 dB to an SINR of -1.4 dB at $P_{Tx} = 23$ dBm. The I-path IMD2 interference is estimated by the IM2RLS using 15 taps, running at the sampling frequency of 30.72 MHz (OSF = 2). This means, the adaptive filter has less taps than the duplexer stop-band impulse response which has 30 complex valued coefficients at OSF = 2. The Q-path IMD2 replica is estimated by a linear 1-tap RLS (running at 30.72 MHz sampling rate) which uses the I-path IMD2 replica as reference input.

The IM2RLS algorithm uses the forgetting-factor $\lambda = 0.9999$ and $\mathbf{P}[-1] = 100\mathbf{I}$ as suggested in [30]. The 1-tap RLS in the Q-path uses the same forgetting factor and the initial coefficient $p[-1] = 1e7$. The coefficient vector of the I-path IM2RLS algorithm is initialized with $\mathbf{w}_1[-1] = [1e-6, 0, 0, \dots, 0]^T$, and the 1-tap RLS with zero. Fig. 7. shows the steady state SINR improvement at different transmit power levels for an IIP2 of +50 dBm. It can be observed, that in both cases (w/o and w/ DC cancellation) the SINR is improved nearly up to the Rx SNR of 3 dB. The convergence behavior at the transmit power of 23 dBm is depicted in Fig. 8. For the

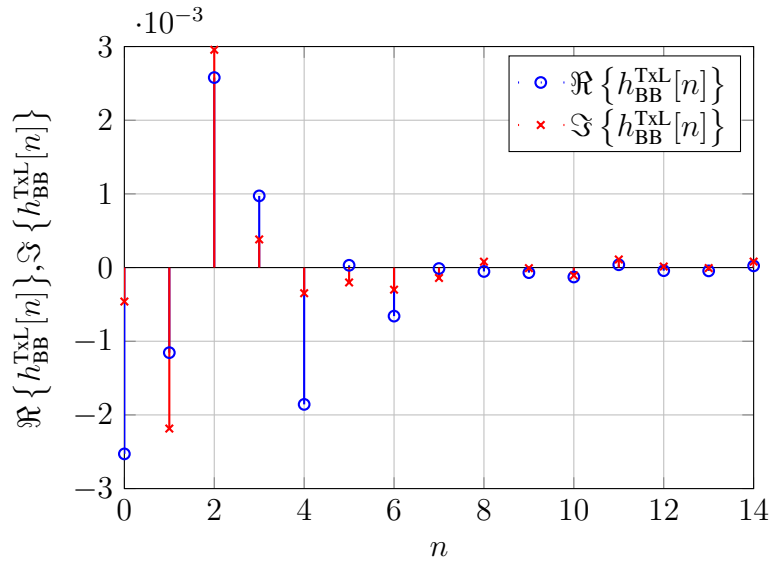


Fig. 6. Real and imaginary part of the 15-tap complex valued duplexer impulse response.

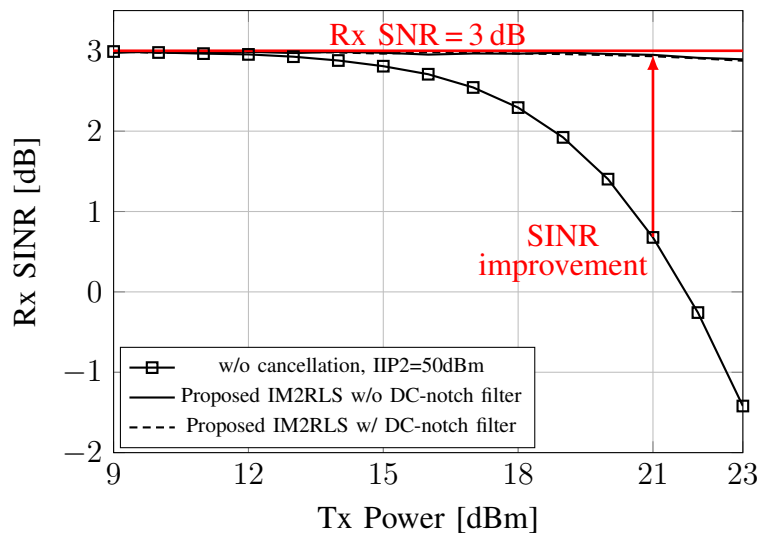


Fig. 7. Improvement of the Rx SINR with the proposed IMD2 cancellation algorithms w/o and w/ using the DC-notch filter at different transmitter power levels. The mixer IIP2 is 50 dBm and the wanted signal at the antenna has a power of $P_{Rx} = -97$ dBm and a SNR of 3 dB.

hypothetical case that the receiver and the IM2RLS are using no DC suppression, the IM2RLS converges faster than with DC suppression. This is reasoned in the additional DC-IMD2 power which supports the algorithm to converge faster. The IIP2 improvement by the digital cancellation

TABLE I
IIP2 IMPROVEMENT BY DIGITAL CANCELLATION

IM2RLS Algorithm	$P_{\text{IMD2}}^{\text{CSF}}$ before	$P_{\text{IMD2}}^{\text{CSF}}$ after	IIP2 after canc.
w/o DC cancellation	-77.5 dBm	-95.8 dBm	68.4 dBm
w/ DC cancellation	-77.5 dBm	-94.5 dBm	67 dBm

is summarized in Table I and may be calculated for the IM2RLS with DC-notch filter via

$$\begin{aligned}
 \text{IIP2}_{\text{after canc.}} &= 2P_{\text{RF}}^{\text{TxL}} - P_{\text{IM2, after canc.}}^{\text{CSF,LTE}} - 13.4 \text{ dB} \\
 &= 2 \cdot (23 \text{ dBm} - 50 \text{ dB} + 20 \text{ dB}) \\
 &\quad + 94.5 \text{ dBm} - 13.4 \text{ dB} = 67 \text{ dBm}.
 \end{aligned} \tag{28}$$

The IIP2 is improved from +50 dBm to 68.4 dBm and 67 dBm by the digital cancellation with the IM2RLS w/o and w/ DC suppression, respectively. The correction factor of 13.4 dB corrects the IMD2 power calculated with the 2-tone formula, to the channel-select, and DC-filtered in-band IMD2 power for the LTE10 full allocation case [6]. For the calculation of the IIP2 improvement, the IMD2 power without DC is used in both cases. The derived IM2RLS algorithm with included DC-notch filter shows an excellent cancellation performance for a full allocated LTE10 transmit signal. However, for small bandwidth allocations like e.g. used in multi-cluster transmissions, the RLS-type algorithm suffers from numerical instability due to the badly-conditioned autocorrelation matrix $\tilde{\mathbf{R}}$. To overcome this limitation, the regularized IM2RLS (R-IM2RLS) is derived in the next section.

V. TIKHONOV REGULARIZATION OF THE NONLINEAR RLS

To reduce the spectral out-of-band (OOB) emission of the LTE signals, not all available subcarriers are allocated. A portion of the subcarriers at the band-edges (guard-band) are forced to zero which introduces correlation in the transmit BB samples. E.g. in a 10 MHz LTE signal a maximum of 600 out of 1024 subcarriers may be occupied by data [31]. This correlation in the Tx BB signal $x_{\text{BB}}[n]$ leads to an badly-conditioned autocorrelation matrix $\mathbf{R} = E \{ \mathbf{x}_{\text{BB}}[n] \mathbf{x}_{\text{BB}}^H[n] \}$ and respectively $\tilde{\mathbf{R}} = E \{ \mathbf{z}_f[n] \mathbf{z}_f^H[n] \}$. Algorithms which need the estimation of the autocorrelation matrix or its inverse $\mathbf{P} = \mathbf{R}^{-1}$ to estimate the system coefficients either iteratively or in batch-mode, are sensitive to the condition number of \mathbf{R} and may suffer from numerical instability if \mathbf{R} is badly-conditioned. Because of this reason, a regularized version of the IM2RLS algorithm (R-IM2RLS) is derived in this section.

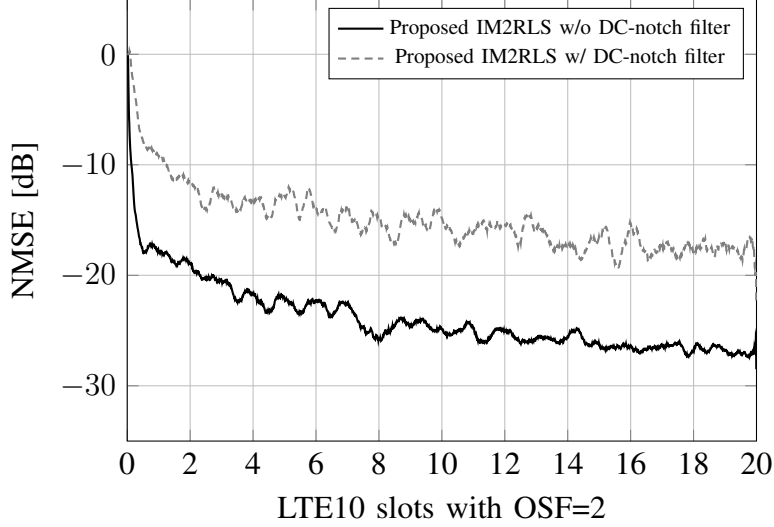


Fig. 8. Convergence of the IM2RLS w/o and w/ DC-notch filter for an LTE transmit signal with 10 MHz bandwidth, OSF of 2 and $P_{Tx} = 23$ dBm. The wanted Rx signal power at the antenna input is $P_{Rx} = -97$ dBm and the Rx SNR = 3 dB. The mixer IIP2 is +50 dBm which corresponds to an Rx SNR desense of 4.4 dB.

A common method to overcome the problem of badly-conditioned autocorrelation matrices is regularization [28]. Adding a positive definite matrix to the estimated auto-correlation matrix in each iteration of the RLS algorithm guarantees that the regularized autocorrelation matrix $\tilde{\mathbf{R}}'$ stays positive definite and maintains therefore the necessary condition for convergence and existence of $\mathbf{P} = \tilde{\mathbf{R}}'^{-1}$ [32].

This method is commonly known as Tikhonov-regularization where a matrix \mathbf{L} is used for the regularization [33]. By including a regularization term in the cost function (15), the new cost function

$$\begin{aligned}
 J'_R[n] &= \sum_{i=0}^n \lambda^{n-i} [|e_I[i]|^2 + \sigma \|\mathbf{L}\mathbf{w}_I[n]\|_2^2] \\
 &= \sum_{i=0}^n \lambda^{n-i} [|e_I[i]|^2 + \sigma \mathbf{w}_I^T[n] \mathbf{L}^T \mathbf{L} \mathbf{w}_I^*[n]]
 \end{aligned} \tag{29}$$

is defined where $e_I[i] = d_I[i] - \mathbf{z}^T[i] \mathbf{w}_I^*[n] * h_s[i]$. The regularization parameter $\sigma \geq 0$ is used to adjust the regularization amount and the real valued matrix \mathbf{L} is typically chosen as $\mathbf{L} = \mathbf{I}$

using the gain vector

$$\mathbf{k}[n] = \frac{\boldsymbol{\Omega}[n]\mathbf{z}_f[n]}{1 + \mathbf{z}_f^H[n]\boldsymbol{\Omega}[n]\mathbf{z}_f[n]}. \quad (37)$$

For the inversion

$$\boldsymbol{\Omega}[n] = [\lambda\mathbf{P}^{-1}[n-1] + \sigma\mathbf{L}^T\mathbf{L}]^{-1}, \quad (38)$$

again the matrix inversion lemma is applied which yields

$$\boldsymbol{\Omega}[n] = \frac{1}{\lambda} (\mathbf{P}[n-1] - \boldsymbol{\Sigma}[n]\mathbf{L}\mathbf{P}[n-1]) \quad (39)$$

where the substitution

$$\boldsymbol{\Sigma}[n] = \sigma\mathbf{P}[n-1]\mathbf{L}^T [\lambda\mathbf{I} + \sigma\mathbf{L}\mathbf{P}[n-1]\mathbf{L}^T]^{-1} \quad (40)$$

is used. After rearranging (40), the expression

$$\begin{aligned} \boldsymbol{\Sigma}[n] &= \frac{\sigma}{\lambda} (\mathbf{P}[n-1] - \boldsymbol{\Sigma}[n]\mathbf{L}\mathbf{P}[n-1]) \mathbf{L}^T \\ &= \sigma\boldsymbol{\Omega}[n]\mathbf{L}^T \end{aligned} \quad (41)$$

is obtained. Unfortunately, the calculation of $\boldsymbol{\Sigma}[n]$ in (40) and therefore $\boldsymbol{\Omega}[n]$ still includes a matrix inversion after applying the matrix inversion lemma. However, by decomposing the matrix $\mathbf{L}^T\mathbf{L}$ in (38) into a sum of V dyads [34]

$$\boldsymbol{\Omega}[n] = \left[\lambda\mathbf{P}^{-1}[n-1] + \sigma \sum_{k=1}^V \mathbf{p}_{k,1}\mathbf{p}_{k,2}^T \right]^{-1}, \quad (42)$$

applying the matrix inversion lemma results in the recursive calculation of (42) via

$$\boldsymbol{\Omega}_k[n] = \boldsymbol{\Omega}_{k-1}[n] - \frac{\boldsymbol{\Omega}_{k-1}[n]\mathbf{p}_{k,1}}{\frac{1}{\sigma} + \mathbf{p}_{k,2}^T\boldsymbol{\Omega}_{k-1}[n]\mathbf{p}_{k,1}} \mathbf{p}_{k,2}^T\boldsymbol{\Omega}_{k-1}[n] \quad (43)$$

for $k = 1 \dots V$ in each iteration n and $\boldsymbol{\Omega}_0[n] = \frac{1}{\lambda}\mathbf{P}[n-1]$. Reformulating (37) yields

$$\mathbf{k}[n] = \mathbf{P}[n]\mathbf{z}_f[n]. \quad (44)$$

The recursive update of the coefficient vector $\mathbf{w}_1[n]$ is obtained by inserting (36), (32), (44), (39) and (41) into $\mathbf{w}_1[n] = \mathbf{P}[n]\tilde{\mathbf{r}}[n]$. The final nonlinear R-IM2RLS algorithm to estimate the I-path IMD2 interference is summarized by (45)-(51):

$$\hat{y}_1[n] = \mathbf{z}^T[n]\mathbf{w}_1^*[n-1] * h_s[n] \quad (45)$$

$$e_1[n] = d_1[n] - \hat{y}_1[n] \quad (46)$$

$$\boldsymbol{\Omega}_k[n] = \boldsymbol{\Omega}_{k-1}[n] - \frac{\boldsymbol{\Omega}_{k-1}[n]\mathbf{p}_{k,1}}{\frac{1}{\sigma} + \mathbf{p}_{k,2}^T\boldsymbol{\Omega}_{k-1}[n]\mathbf{p}_{k,1}} \mathbf{p}_{k,2}^T\boldsymbol{\Omega}_{k-1}[n] \quad (47)$$

$$\mathbf{k}[n] = \frac{\boldsymbol{\Omega}_V[n]\mathbf{z}_f[n]}{1 + \mathbf{z}_f^H[n]\boldsymbol{\Omega}_V[n]\mathbf{z}_f[n]}. \quad (48)$$

$$\mathbf{P}[n] = \boldsymbol{\Omega}_V[n] - \mathbf{k}[n]\mathbf{z}_f^H[n]\boldsymbol{\Omega}_V[n] \quad (49)$$

$$\boldsymbol{\Sigma}[n] = \sigma\boldsymbol{\Omega}_V[n]\mathbf{L}^T \quad (50)$$

$$\mathbf{w}_I[n] = [\mathbf{I} - (\mathbf{I} - \mathbf{k}[n]\mathbf{z}_f^H[n])\boldsymbol{\Sigma}[n]\mathbf{L}] \mathbf{w}_I[n-1] + \mathbf{k}[n]e_I[n] \quad (51)$$

The proposed algorithm is initialized with $\mathbf{w}_I[-1] \neq \mathbf{0}$, $0 \ll \lambda \leq 1$ and $\mathbf{P}[-1] = \nu\mathbf{I}$ with $\nu > 0$. When the DC suppression is used, then the R-IM2RLS update equations become (52)-(59):

$$\hat{y}_I[n] = \mathbf{z}^T[n]\mathbf{w}_I^*[n-1] * h_s[n] \quad (52)$$

$$\hat{y}_{AC,I}[n] = 0.998\hat{y}_{AC,I}[n-1] + \hat{y}_I[n] - \hat{y}_I[n-1] \quad (53)$$

$$e_{AC,I}[n] = d_{AC,I}[n] - \hat{y}_{AC,I}[n] \quad (54)$$

$$\boldsymbol{\Omega}_k[n] = \boldsymbol{\Omega}_{k-1}[n] - \frac{\boldsymbol{\Omega}_{k-1}[n]\mathbf{p}_{k,1}}{\frac{1}{\sigma} + \mathbf{p}_{k,2}^T\boldsymbol{\Omega}_{k-1}[n]\mathbf{p}_{k,1}} \mathbf{p}_{k,2}^T\boldsymbol{\Omega}_{k-1}[n] \quad (55)$$

$$\mathbf{k}[n] = \frac{\boldsymbol{\Omega}_V[n]\mathbf{z}_f[n]}{1 + \mathbf{z}_f^H[n]\boldsymbol{\Omega}_V[n]\mathbf{z}_f[n]}. \quad (56)$$

$$\mathbf{P}[n] = \boldsymbol{\Omega}_V[n] - \mathbf{k}[n]\mathbf{z}_f^H[n]\boldsymbol{\Omega}_V[n] \quad (57)$$

$$\boldsymbol{\Sigma}[n] = \sigma\boldsymbol{\Omega}_V[n]\mathbf{L}^T \quad (58)$$

$$\begin{aligned} \mathbf{w}_I[n] &= [\mathbf{I} - (\mathbf{I} - \mathbf{k}[n]\mathbf{z}_f^H[n])\boldsymbol{\Sigma}[n]\mathbf{L}] \mathbf{w}_I[n-1] \\ &+ \mathbf{k}[n]e_{AC,I}[n] \end{aligned} \quad (59)$$

The DC-notch filter (53) is used to remove the DC from the IMD2 replica (52). The complexity of the R-IM2RLS with DC-notch filter and $L = \sigma\mathbf{I}$ is $8N_w^3 + 21N_w^2 + 5N_{CSF} + 18N_w + 1$ real multiplications and $2N_w^2 + 2N_w$ real divisions per iteration.

VI. SIMULATION ENVIRONMENT

The performance of the R-IM2RLS algorithm with the three above mentioned regularization matrices \mathbf{L} is evaluated with an FDD scenario using an LTE10 multi-cluster intra-band Tx signal which has a native sampling frequency of $f_s = 15.36$ MHz, QPSK modulation and short cyclic prefix. The IMD2 interference in the I-path is estimated by the R-IM2RLS, while the Q-path IMD2 is estimated by a linear 1-tap RLS which uses the I-path IMD2 replica as reference input. The resulting multi-cluster TxL signal has a strong frequency-selectivity like indicated in Fig. 9. The R-IM2RLS in the I-path has 15 taps and runs on the higher sampling rate of 30.72 MHz due to the OSF of 2. This means, the adaptive filter has less taps than the impulse response which is estimated. The linear 1-tap Q-path RLS runs also on the sampling rate of 30.72 MHz. The received signal $d[n]$ is DC filtered and the proposed algorithm is using the DC-notch filter to suppress the DC of the IMD2 replica signal. The wanted Rx signal has a power of $P_{\text{Rx}} = -97$ dBm at the antenna with an SNR of 3 dB. The assumed Rx mixer IIP2 is +60 dBm which corresponds to an Rx SNR desense of 1 dB for the specific intra-band multi-cluster transmit signal at 23 dBm power level. The thermal noise floor of the receiver is assumed at -104.5 dBm per 10 MHz and the receiver NF is 4.5 dB. The resulting receiver noise floor and Rx power with 20 dB LNA gain is at -80 dBm $\hat{=}$ -108.2 dBm/15 kHz and -77 dBm respectively. The spectrum of the signals at $P_{\text{Tx}} = 23$ dBm is depicted in Fig. 9. It can be observed, that the resulting IMD2 interference $y_{\text{BB}}^{\text{IMD2}}$ is mostly below the receiver noise floor but still leads to an SNR degradation of 1 dB. The depicted interference replica is estimated by the R-IM2RLS with the regularization $\mathbf{L} = 3e - 7 \mathbf{I}$. The multi-cluster LTE10 Tx signal uses 21/50 RBs (252 subcarriers from 1024), which means hat 3.78 MHz of the available 9.015 MHz are allocated. With an OSF of 2 this corresponds to an allocated bandwidth-to-sampling-rate ratio of $3.78/30.72 = 0.12$ which introduces a high correlation in the transmit BB samples. The resulting condition number $\text{cond}(\tilde{\mathbf{R}})$ of the 15×15 dimensional autocorrelation matrix $\tilde{\mathbf{R}} = E \{ \mathbf{z}_f \mathbf{z}_f^H \}$ is in the order of 10^7 which results in a bad conditioned estimation, and may lead to numerical problems. The regularization of the R-IM2RLS improves numerical estimation of the matrix $\mathbf{P}[n]$ by lowering the condition number of the regularized matrix $\tilde{\mathbf{R}}'$.

A. IMD2 Self-Interference of a Multi-Cluster Tx Signal

For the estimation of the resulting IMD2 interference bandwidth, the bandwidth between the minimum and maximum allocated subcarrier in the multi-cluster Tx signal is of interest. In the

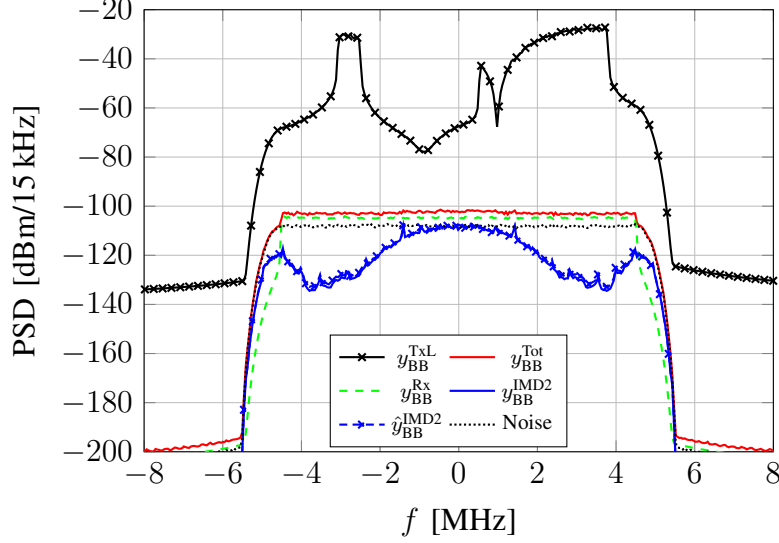


Fig. 9. Equivalent BB spectrum of the frequency-selective Tx leakage signal $y_{\text{BB}}^{\text{TxL}}$ (the corresponding passband signal is located at f_{Tx}) and the total received signal $y_{\text{BB}}^{\text{Tot}}$ after amplification with 20 dB LNA gain. The wanted Rx signal with SNR=3 dB, and the receiver noise floor after amplification with 20 dB LNA gain are at -77 dBm and -80 dBm $\hat{=}$ -108.2 dBm/15 kHz respectively. The total received signal contains the DC-, and channel-select filtered IMD2 interference at $P_{\text{Tx}} = 23$ dBm and the IIP2 is 60 dBm. used clustered LTE10 transmit signal the allocated RBs are $\{9 - 11, 29 - 46\}$ with a numbering from left to right and the total number of 50 RBs. For the IMD2 bandwidth estimation the resulting bandwidth between the lowest allocated subcarrier (RB 9) and the upper edge (RB 46) of the allocated RBs is $(3 + 17 + 18) \cdot 12 \cdot 15$ kHz = 6.84 MHz. Each RB has 12 subcarriers and 15 kHz subcarrier spacing. The resulting IMD2 interference bandwidth is 2×6.84 MHz = 13.68 MHz which means that a small portion of the IMD2 interference is suppressed by the CSF. The full IMD2 interference including the DC, the IMD2 interference after the CSF and DC-removal, and the estimated IMD2 replica are visualized in Fig. 10. It can be observed, that the R-IM2RLS is able to estimate the IMD2 interference down to 20 dB below the receiver noise floor.

B. Numerical Simulation Results

In the following simulation results, the IMD2 self-interference cancellation performance in case of an intra-band multi-cluster Tx signal, using the R-IM2RLS algorithm (52)-(59) using the DC-notch filter with different regularization matrices is evaluated. The forgetting factor of the R-IM2RLS is chosen as $\lambda = 0.9999$, $\mathbf{P}[-1] = 100\mathbf{I}$, and the regularization constant $\sigma = 3e - 7$. The 1-tap RLS in the Q-path uses the same forgetting factor but the initial coefficient $p[-1] =$

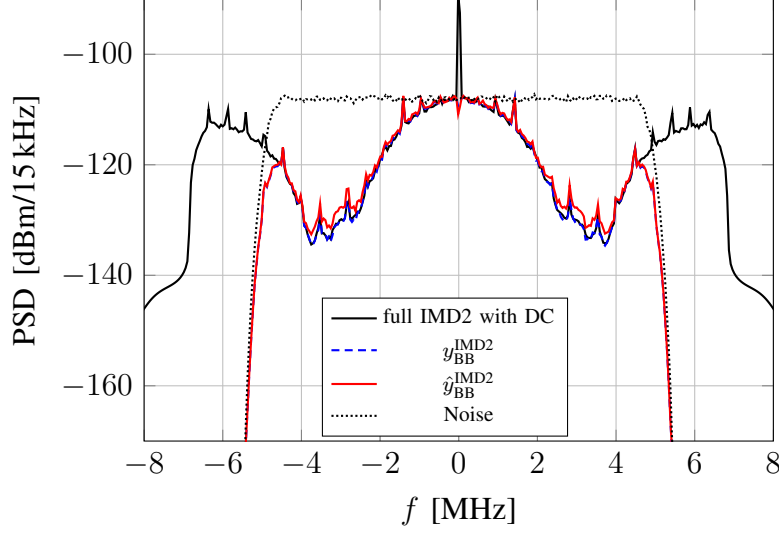


Fig. 10. Generated IMD2 interference with the bandwidth of 13.68 MHz at $P_{Tx} = 23$ dBm. The resulting in-band BB IMD2 interference y_{BB}^{IMD2} after the CSF and DC-removal is below the receiver noise floor. The R-IM2RLS estimates the IMD2 interference down to 20 dB below the noise floor.

1e7. The coefficient vector of the R-IM2RLS is initialized with $\mathbf{w}_1[-1] = [1e-6, 0, 0, \dots, 0]^T$ for the I-path, and the 1-tap Q-path RLS is initialized with zero. The performance is evaluated for the different regularization matrices $\mathbf{L} = 3e-7 \mathbf{I}$ (Tikhonov regularization), $\mathbf{L} = 3e-7$ upperbidiag(1, -1) (first order derivative smoothing matrix), and $\mathbf{L} = 3e-7$ diag(1, -2, 1) (second order derivative smoothing matrix). The IM2RLS without regularization is not included in the comparison due to numerical instability reasoned by the extremely high condition number of $\tilde{\mathbf{R}}$ which is in the order of 10^7 . The performance of the R-IM2RLS is compared with the recently published LMS-type algorithm (IM2LMS) [6]. The IM2LMS uses the step-size $\mu = 0.005$, the regularization parameter $\gamma = 0.001$, and the initial coefficient vector $\hat{\mathbf{w}}_1[-1] = [1e-4, 0, 0, \dots, 0]^T$. The Q-path IMD2 replica is estimated by a linear normalized 1-tap LMS which uses the I-path IMD2 replica estimated by the IM2LMS as reference input. The normalized 1-tap LMS uses a step-size of 1, the regularization parameter is set to 1e-7 and the initial coefficient is set to zero. The value of the step-size is set to the best compromise between steady-state cancellation and convergence time. The convergence of the algorithms is compared using the ensemble normalized mean-square-error (NMSE), and the steady-state cancellation by the SINR. The SINR improvement of the Rx signal for the different algorithms and regularizations is depicted in Fig. 11. The convergence behaviour of the algorithms is depicted in Fig. 12. The R-IM2RLS shows a faster initial convergence than the IM2LMS algorithm which takes about twice as long to reach an NMSE of -10 dB. The

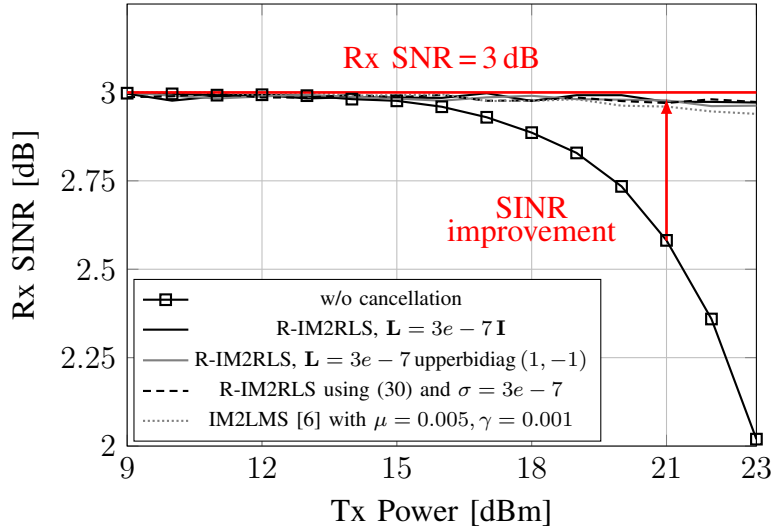


Fig. 11. Improvement of the Rx SINR at different transmitter power levels and an Rx mixer IIP2 of +60 dBm. The algorithms are using the DC-filtered receive signal, and the R-IM2RLS/IM2LMS algorithms are using the DC-notch filter to remove the DC. The wanted signal at the antenna has the power $P_{R_x} = -97$ dBm and a SNR of 3 dB.

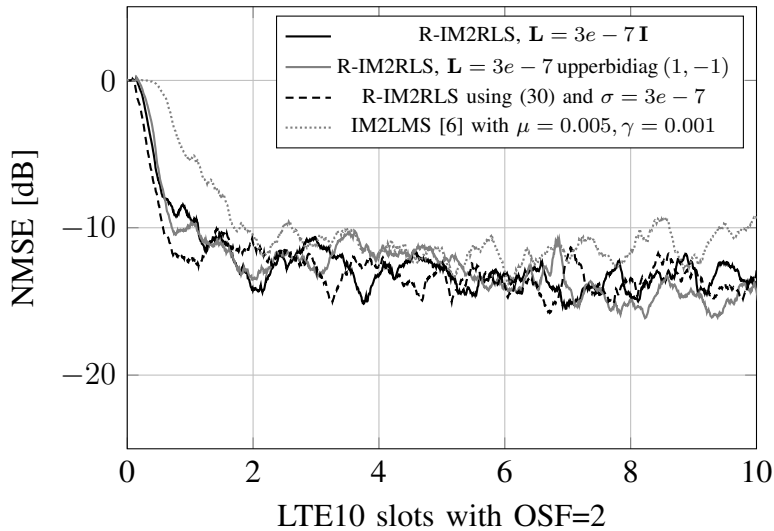


Fig. 12. Convergence of the R-IM2RLS with different regularization matrices and the IM2LMS algorithm at the transmit power level of $P_{T_x} = 23$ dBm. The algorithms are using the DC-notch filter to suppress the DC.

evolution of the condition number of $\tilde{\mathbf{R}}'[n] = \mathbf{P}[n]^{-1}$ is illustrated in Fig. 13. The condition number of $\tilde{\mathbf{R}}$ estimated by the IM2RLS without regularization drastically increases up to values between 10^7 and 10^8 . In contrast to that, the condition number of $\tilde{\mathbf{R}}'$ estimated by the R-IM2RLS with different regularization matrices \mathbf{L} stays below 400 for the specific clustered Tx example. The achieved IIP2 after the digital IMD2 cancellation is summarized in Table II. The R-IM2RLS

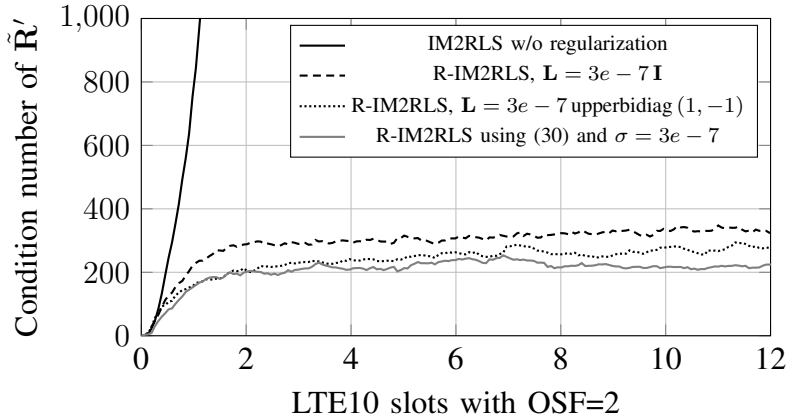


Fig. 13. Evolution of the condition number of $\tilde{\mathbf{R}}'[n] = \mathbf{P}^{-1}[n]$ for a clustered allocation like depicted in Fig. 9 and 23 dBm transmit power. The condition number of $\tilde{\mathbf{R}} = E\{\mathbf{z}\mathbf{z}^H\}$ without regularization is in the order of 10^7 to 10^8 .

and IM2LMS algorithms are improving the IIP2 from 60 dBm to about 77 dBm and 73 dBm, respectively.

TABLE II
IIP2 IMPROVEMENT BY DIGITAL CANCELLATION FOR THE CLUSTERED TX SIGNAL

Algorithm	IIP2 after canc.
R-IM2RLS, $\mathbf{L} = 3e - 7 \mathbf{I}$	77.2 dBm
R-IM2RLS, $\mathbf{L} = 3e - 7$ upperbidiag(1, -1)	76.5 dBm
R-IM2RLS using (30) and $\sigma = 3e - 7$	76.4 dBm
IM2LMS	73 dBm

VII. VERIFICATION OF THE DERIVED ALGORITHM WITH MEASUREMENT DATA

The proposed R-IM2RLS algorithm is evaluated with measurement data and Matlab post-processing. The measurement setup (A) depicted in Fig. 14 includes the LTE band 2 duplexer model B8663 from TDK, the LNA ZX60-2534MA+ with 41.3 dB gain and 2.6 dB NF and the ZAM-42 Level 7 mixer which has 25 dB RF-to-LO terminal isolation. The measurement is carried out for the I-path mixer and a full allocated LTE-A transmit signal with 10 MHz bandwidth, QPSK modulation and short cyclic prefix. The transmit frequency is set to $f_{Tx} = 1.855$ GHz and the mixer LO frequency is $f_{Rx} = 1.935$ GHz (80 MHz duplexing distance). The LTE transmit signal is generated with the R&S SMW 200A signal generator (B), and the TxL signal which leaks into the receiver with 80 MHz frequency offset to the LO signal is amplified by the LNA

gain. This amplified TxL signal generates the BB IMD2 interference at the output of the I-path mixer which is measured with the real-time oscilloscope RTO 1044 (C). The TxL signal after the LNA is measured by the R&S FSW26 spectrum analyzer (D), and the LO signal with 7 dBm for the ZAM-42 mixer is generated by the R&S SMB 100A signal generator (E). The transmit

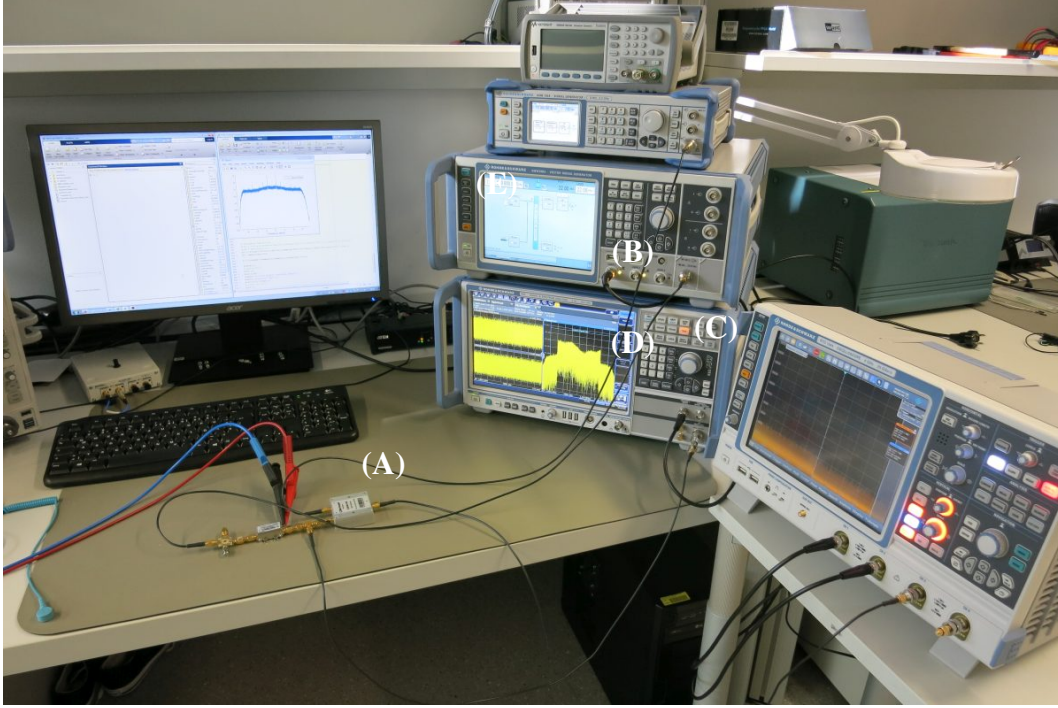


Fig. 14. Measurement setup including the DUT (A) with the LNA ZX60-2534MA+, the mixer ZAM-42 from Mini Circuits and the LTE band 2 duplexer B8663. The signal generator R&S SMW 200A (B) generates the LTE transmit signal and the R&S real-time oscilloscope RTO 1044 (C) is used to measure the BB signal after the mixer. The R&S FSW26 spectrum analyzer (D) is used to measure the TxL signal, and the signal generator R&S SMB 100A (E) generates the mixer LO signal.

power is set to $P_{\text{RF}}^{\text{Tx}} = 19.3 \text{ dBm}$, which leads in combination with the duplexer attenuation of 67.6 dB (at $f_{\text{Tx}} = 1.855 \text{ GHz}$) and the LNA gain of 41.3 dB to the typical TxL signal power of $P_{\text{RF}}^{\text{TxL}} = 19.3 \text{ dBm} - 67.6 \text{ dB} + 41.3 \text{ dB} = -7 \text{ dBm}$. The measured I-path mixer BB output data stream and the complex valued BB transmit samples are used for the Matlab post-processing. The spectrum of the signals before and after digital cancellation with the R-IM2RLS using a Tikhonov regularization and the parameters $\mathbf{P}[-1] = 10\mathbf{I}$, $\lambda = 0.99999$ and $\mathbf{L} = 1e - 5\mathbf{I}$ are depicted in Fig. 15. The Matlab post-cancellation showed that 10 taps were sufficient to cancel the IMD2 interference by 2.2 dB down to the noise floor. The coefficient vector was initialized with $\mathbf{w}_1[-1] = [1e - 6, 0, 0, \dots, 0]^T$, and the convergence of the coefficients is shown in Fig. 16 which indicates that the coefficients converged after about 5 LTE symbols.

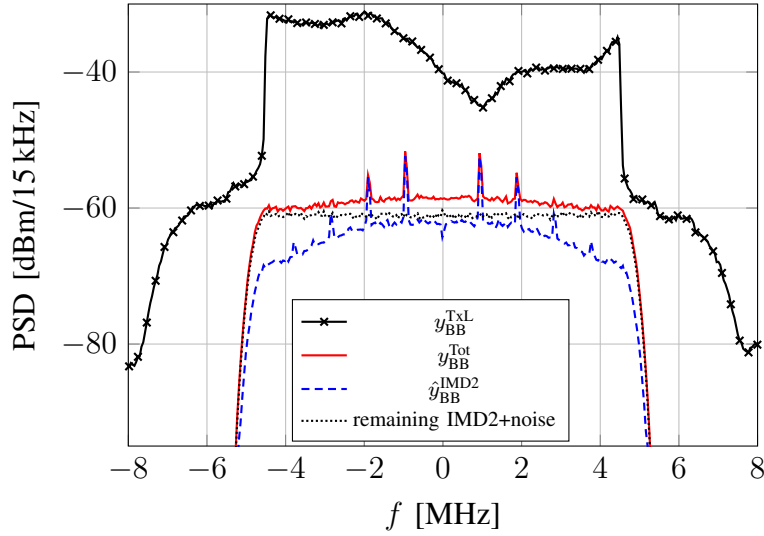


Fig. 15. Spectrum of the measured TxL signal y_{BB}^{TxL} and the receive signal y_{BB}^{Tot} including noise and the IMD2 interference. The BB equivalent TxL signal shows a strong frequency selectivity. Also shown are the spectrum of the estimated IMD2 replica \hat{y}_{BB}^{IMD2} and the remaining IMD2 and noise after the cancellation.

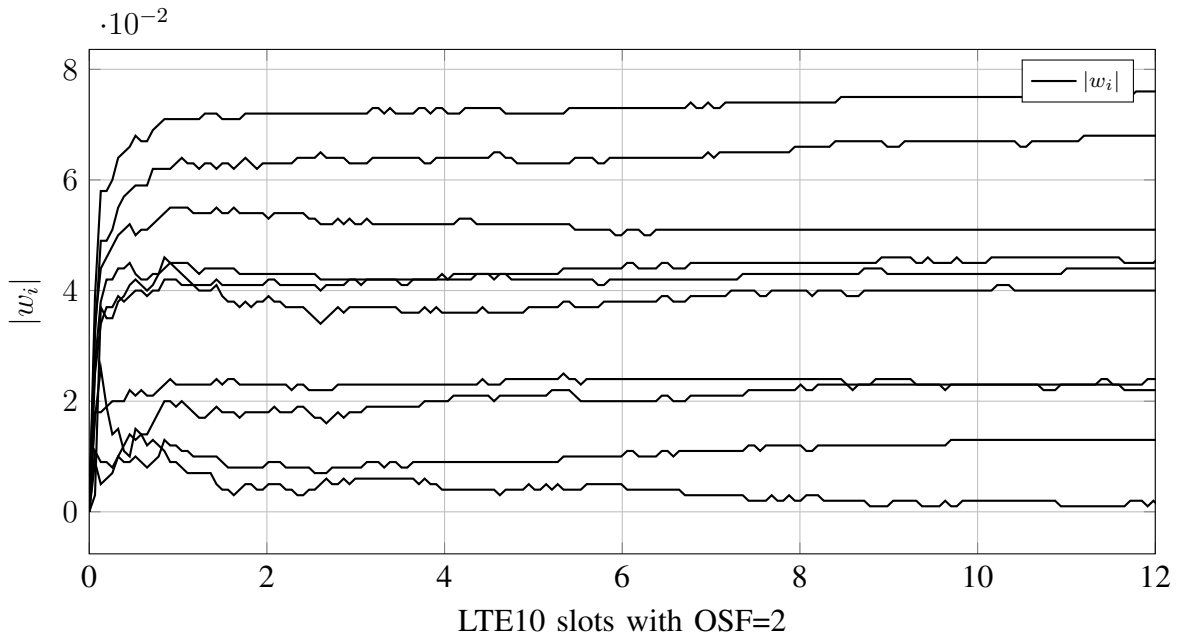


Fig. 16. Evolution of the estimated coefficients by the R-IM2RLS.

VIII. CONCLUSION

This paper presented a novel nonlinear RLS type adaptive filter (IM2RLS) and its robust version (R-IM2RLS) for the digital IMD2 self-interference cancellation in LTE FDD RF transceivers. The R-IM2RLS provides stability and numerical tractability for highly correlated transmit signals

which may result in an ill-conditioned autocorrelation matrix. The proposed R-IM2RLS is able to cancel the IMD2 interference generated by a highly frequency-selective Tx leakage signal, and its performance is evaluated with different regularization matrices. Typical RF receivers use a DC cancellation to prevent the ADC from saturation and a CSF to limit the signal bandwidth. Therefore the IMD2 interference which is generated by the second-order nonlinearity in the mixer is DC filtered and its bandwidth is reduced to the LTE signal bandwidth. Consequently, the adaptive filter needs to provide a DC-filtered in-band IMD2 replica. This contribution shows that the IM2RLS/R-IM2RLS adaptive filter is able to reproduce the in-band IMD2 interference without DC by including the CSF and a DC-notch filter within the algorithm. It is shown, that the proposed algorithm may have multiple solutions of the estimated coefficient vector because of the envelope-squaring nature of the IMD2 interference. The algorithm converges within a few LTE symbols and the steady-state Rx SNR degradation by the IMD2 self-interference in case of a multi-cluster transmit signal is improved in simulation from 1 dB to less than 0.05 dB. The performance of the R-IM2RLS is proved in an LTE measurement scenario with discrete RF components. The IMD2 interference in the received signal is canceled to the noise floor and a convergence of the coefficients within 5 LTE symbols is achieved.

ACKNOWLEDGMENT

The authors wish to acknowledge DMCE GmbH & Co KG, an Intel subsidiary for supporting this work carried out at the Christian Doppler Laboratory for Digitally Assisted RF Transceivers for Future Mobile Communications. The financial support by the Austrian Federal Ministry of Science, Research and Economy and the National Foundation for Research, Technology and Development is gratefully acknowledged.

REFERENCES

- [1] Ericsson and ST-Ericsson, "R4-126964, REFSENS with one UL carrier for NC intra-band CA," Ericsson, Tech. Rep., November 2012. [Online]. Available: http://www.3gpp.org/ftp/tsg_ran/WG4_Radio/TSGR4_65/docs/R4-126964.zip
- [2] R. Vazny, W. Schelmbauer, H. Pretl, S. Herzinger, and R. Weigel, "An interstage filter-free mobile radio receiver with integrated TX leakage filtering," In *2010 IEEE Radio Frequency Integrated Circuits Symposium*, May 2010, pp. 21–24.
- [3] A. Gebhard, R. Kanumalli, B. Neurauder, and M. Huemer, "Adaptive Self-Interference Cancellation in LTE-A Carrier Aggregation FDD Direct-Conversion Transceivers," In *Proceedings of the 9th IEEE Sensor Array Multichannel Signal Processing Conference (SAM 2016)*, July 2016.
- [4] R. Kanumalli, A. Gebhard, A. Elmaghraby, A. Mayer, D. Schwarty, and M. Huemer, "Active Digital Cancellation of Transmitter Induced Modulated Spur Interference in 4G LTE Carrier Aggregation Transceivers," In *Proceedings of the 83rd Vehicular Technology Conference (VTC Spring)*, 2016.

- [5] B. Razavi, "Design considerations for direct-conversion receivers," In *IEEE Transactions on Circuits and Systems II: Analog and Digital Signal Processing*, Vol. 44, No. 6, pp. 428–435, Jun 1997.
- [6] A. Gebhard, C. Motz, R. Kanumalli, H. Pretl, and M. Huemer, "Nonlinear Least-Mean-Squares Type Algorithm for Second-Order Interference Cancellation in LTE-A RF Transceivers," In Proceedings of the *51st Asilomar Conference on Signals, Systems, and Computers*, 2017.
- [7] A. Kiayani, L. Anttila, and M. Valkama, "Modeling and dynamic cancellation of TX-RX leakage in FDD transceivers," In Proceedings of the *56th International Midwest Symposium on Circuits and Systems (MWSCAS)*, Aug 2013, pp. 1089–1094.
- [8] C. Lederer and M. Huemer, "LMS Based Digital Cancellation of Second-Order TX Intermodulation Products in Homodyne Receivers," In Proceedings of the *Radio and Wireless Symposium (RWS)*, Jan 2011, pp. 207–210.
- [9] A. Frotzschner and G. Fettweis, "A Stochastic Gradient LMS Algorithm for Digital Compensation of Tx Leakage in Zero-IF-Receivers," In Proceedings of the *Vehicular Technology Conference (VTC Spring 2008)*, May 2008, pp. 1067–1071.
- [10] M. Kahrizi, J. Komaili, J. E. Vasa, and D. Agahi, "Adaptive filtering using LMS for digital TX IM2 cancellation in WCDMA receiver," In Proceedings of the *IEEE Radio and Wireless Symposium*, Jan 2008, pp. 519–522.
- [11] A. Frotzschner and G. Fettweis, "Least Squares Estimation for the Digital Compensation of Tx Leakage in zero-IF Receivers," In Proceedings of the *Global Telecommunications Conference (GLOBECOM 2009)*, Nov 2009, pp. 1–6.
- [12] H. Gheidi, H. T. Dabag, Y. Liu, P. M. Asbeck, and P. Gudem, "Digital cancellation technique to mitigate receiver desensitization in cellular handsets operating in carrier aggregation mode with multiple uplinks and multiple downlinks," In Proceedings of the *IEEE Radio and Wireless Symposium (RWS)*, Jan 2015, pp. 221–224.
- [13] V. J. Mathews and G. L. Sicuranza, *Polynomial signal processing*. Wiley-Interscience, 2000, Vol. 27.
- [14] C. Lederer and M. Huemer, "Simplified complex LMS algorithm for the cancellation of second-order TX intermodulation distortions in homodyne receivers," In Proceedings of the *Forty Fifth Asilomar Conference on Signals, Systems and Computers (ASILOMAR)*, Nov 2011, pp. 533–537.
- [15] C. W. Liu and M. Damgaard, "IP2 and IP3 nonlinearity specifications for 3G/WCDMA receivers," In *High Frequency Electronics*, pp. 16–29, 2009.
- [16] A. Walid, "Effective IM2 products estimation for two-tone and W-CDMA modulated blockers in 3GPP direct-conversion receivers."
- [17] E. S. Atalla, A. Bellaouar, and P. T. Balsara, "IIP2 requirements in 4G LTE handset receivers," In Proceedings of the *56th International Midwest Symposium on Circuits and Systems (MWSCAS)*, Aug 2013, pp. 1132–1135.
- [18] 3GPP, "Evolved Universal Terrestrial Radio Access (E-UTRA); User Equipment (UE) radio transmission and reception," 3GPP, Tech. Rep., May 2015. [Online]. Available: http://www.3gpp.org/ftp/specs/archive/36_series/36.101/36101-bg0.zip
- [19] I. Madadi, M. Tohidian, K. Cornelissens, P. Vandenameele, and R. B. Staszewski, "A High IIP2 SAW-Less Superheterodyne Receiver With Multistage Harmonic Rejection," In *IEEE Journal of Solid-State Circuits*, Vol. 51, No. 2, pp. 332–347, Feb 2016.
- [20] K. Dufrene, Z. Boos, and R. Weigel, "Digital Adaptive IIP2 Calibration Scheme for CMOS Downconversion Mixers," In *IEEE Journal of Solid-State Circuits*, Vol. 43, No. 11, pp. 2434–2445, Nov 2008.
- [21] A. V. Oppenheim, R. W. Schaffer, and J. R. Buck, *Discrete-time signal processing*. Prentice Hall, 1999, Vol. 2.
- [22] R. Tzschoppe and J. B. Huber, "Causal discrete-time system approximation of non-bandlimited continuous-time systems by means of discrete prolate spheroidal wave functions," In *European Transactions on Telecommunications*, Vol. 20, No. 6, pp. 604–616, Aug 2008.
- [23] D. H. Brandwood, "A complex gradient operator and its application in adaptive array theory," In *Communications, Radar and Signal Processing, IEE Proceedings F*, Vol. 130, No. 1, pp. 11–16, Feb 1983.

- [24] A. van den Bos, "Complex gradient and Hessian," In *IEE Proceedings - Vision, Image and Signal Processing*, Vol. 141, No. 6, pp. 380–383, Dec 1994.
- [25] D. P. Mandic and V. S. L. Goh, *Complex valued nonlinear adaptive filters: noncircularity, widely linear and neural models*. John Wiley & Sons, 2009, Vol. 59.
- [26] Y. Chen, T. Le-Ngoc, B. Champagne, and C. Xu, "Recursive least squares constant modulus algorithm for blind adaptive array," In *IEEE Transactions on Signal Processing*, Vol. 52, No. 5, pp. 1452–1456, May 2004.
- [27] Y. X. Chen, Z. Y. He, T. S. Ng, and P. C. K. Kwok, "RLS adaptive blind beamforming algorithm for cyclostationary signals," In *Electronics Letters*, Vol. 35, No. 14, pp. 1136–1138, Jul 1999.
- [28] A. H. Sayed, *Fundamentals of adaptive filtering*. John Wiley & Sons, 2003, Vol. 1.
- [29] P. Schreier and L. L. Scharf, *Statistical Signal Processing of Complex-Valued Data: The Theory of Improper and Noncircular Signals*. Cambridge University Press, 2010.
- [30] R. Isermann, *Identifikation dynamischer Systeme 1*. Springer-Verlag, 1991, Vol. 2.
- [31] R. Ferrs and O. Sallent, *Mobile Broadband Communications for Public Safety: The Road Ahead Through LTE Technology*. Wiley, 2015, Vol. 1.
- [32] S. Gunnarsson, "Combining tracking and regularization in recursive least squares identification," In *Proceedings of 35th IEEE Conference on Decision and Control*, Vol. 3, Dec 1996, pp. 2551–2552 vol.3.
- [33] T. Huckle and M. Sedlacek, "Data Based Regularization Matrices for the Tikhonov-Phillips Regularization," In *Proceedings of the Applied Mathematics and Mechanics (PAMM)*, Vol. 12, No. 1. Wiley Online Library, 2012, pp. 643–644.
- [34] J. Dokoupil and V. Burlak, "Variable Regularized Square Root Recursive Least Square Method," In *11th IFAC*, Vol. 45, No. 7, pp. 78 – 82, 2012, iEEE International Conference on Programmable Devices and Embedded Systems.